

Supplementary information for

An anti-thermal-quenching organic-inorganic hybrid manganese-based single-crystal scintillator for high-temperature X-ray imaging

Jing-Hua Chen, Jian-Bin Luo, Zi-Lin He, Qing-Peng Peng, Jun-Hua Wei*, Zhi-Zhong Zhang, Xiu-Xian Guo and
Dai-Bin Kuang*

Key Laboratory of Bioinorganic and Synthetic Chemistry of Ministry of Education, Lehn Institute of Functional Materials, GBRCE for Functional Molecular Engineering, School of Chemistry, IGCME, Sun Yat-Sen University, Guangzhou 510275, China.

*Corresponding Author: weijh39@mail.sysu.edu.cn, kuangdb@mail.sysu.edu.cn

Table of contents

Supplementary Figures

Supplementary Scheme 1. Synthesis routes of 4-NH₃TBPBr and 4-DMATBPBr crystals.

Supplementary Scheme 2. Schematic diagram of the synthesis route of large-size (4-DMATBP)MnBr₄ single crystal.

Fig. S1. Physical characterization of the as-synthesized 4-NH₃TBPBr crystal.

Fig. S2. Physical characterization of the as-synthesized 4-DMATBPBr crystal.

Fig. S3. Single-crystal structure of the as-synthesized organic compounds.

Fig. S4. Thermal properties of the as-synthesized phosphonium salts.

Fig. S5. The asymmetric units of (4-NH₃TBP)MnBr₄ and (4-DMATBP)MnBr₄ crystal.

Fig. S6. Thermal properties of the as-synthesized metal halide crystals.

Fig. S7. Optical properties of as-synthesized compounds.

Fig. S8. Photoluminescence properties of the as-synthesized Mn-based crystal.

Fig. S9. The decay lifetime of two single crystals.

Fig. S10. Photoluminescence properties and PLQY of Mn-based crystals.

Fig. S11. Temperature-dependent RL spectrum of (4-NH₃TBP)MnBr₄ and (4-DMATBP)MnBr₄ crystal.

Fig. S12. The Mini-X2 silver (Ag) output spectrum collected at 40 kV.

Fig. S13. RL response under different X-ray dose rates.

Fig. S14. 3D packing diagrams for (4-NH₃TBP)MnBr₄ and (4-DMATBP)MnBr₄ crystal viewed along the a-axis.

Fig. S15. The 2D fingerprint patterns for C–H...Br H–bond of [MnBr₄]²⁻ in (4-NH₃TBP)MnBr₄, (4-DMATBP)MnBr₄ and (TPPen)₂MnBr₄ crystal.

Fig. S16. Temperature-dependent PL decay curves of (4-DMATBP)MnBr₄ crystal.

Fig. S17. EPR spectra of 4-NH₃TBPBr and (4-NH₃TBP)MnBr₄ crystal.

Fig. S18. Experimental and the fitted plot of EPR spectra for (4-DMATBP)MnBr₄ single crystal.

Fig. S19. Schematic diagram of the possible vacancy-defect structures in (4-DAMTBP)MnBr₄ crystal.

Fig. S20. The density of states and projected density of states of (4-DMATBP)MnBr₄ crystal with different structure defects.

Fig. S21. Energy level diagram of pure (4-DAMTBP)MnBr₄ crystal and possible vacancy defects.

Fig. S22. Ultraviolet-visible transmittance spectra of (4-NH₃TBP)MnBr₄ wafer and (4-DMATBP)MnBr₄ wafer.

Fig. S23. X-ray imaging of the (4-NH₃TBP)MnBr₄ and (4-DMATBP)MnBr₄ wafers.

Fig. S24. The gray value changes of the X-ray imaging of the (4-DMATBP)MnBr₄ crystal at different temperatures.

Fig. S25. X-ray images of electronic component B and electronic chip using the (4-DMATBP)MnBr₄ crystal at different temperatures.

Fig. S26. X-ray imaging of LuAG:Ce scintillator.

Fig. S27. The irradiation stability of (4-DMATBP)MnBr₄ crystal under X-ray irradiation with a total dosage of 133 Gy.

Supplementary Tables

Table S1. The crystal structure data of 4-NH₃TBPBr, (4-NH₃TBP)MnBr₄, 4-DMATBPBr, and (4-DMATBP)MnBr₄.

Table S2. The thermal properties of the as-synthesized phosphonium salts.

Table S3. The Mn-Br bond lengths and shortest Mn-Mn distances of (4-NH₃TBP)MnBr₄ crystal and (4-DMATBP)MnBr₄ crystal.

Table S4. The thermal properties of the as-synthesized Mn-based halides.

Table S5. The Mn...H(Y)–C (N) bond lengths between [MnBr₄]²⁻ and organic cations in (4-NH₃TBP)MnBr₄ crystal.

Table S6. The Mn...H(Y)–C (N) bond lengths between [MnBr₄]²⁻ and organic cations in (4-DMATBP)MnBr₄ crystal.

Table S7. The crystal structure data of (4-DMATBP)MnBr₄ crystal at different temperatures.

Table S8. The crystal volume and shortest Mn-Mn distance of (4-DMATBP)MnBr₄ crystal at different temperatures.

Table S9. The average PL lifetimes of (4-DMATBP)MnBr₄ crystal at different temperatures.

Supplemental experimental procedures

Materials.

Triphenylphosphine (TPP, >99%, Aladdin), 4-bromo-1-butanamine hydrobromide (96%, Bidepharm), (4-Bromobutyl)triphenylphosphonium (4-BrTBP, 97%, Bidepharm), dimethylamine solution (AR, 40 wt% in water, Aladdin), manganese bromide tetrahydrate ($\text{MnBr}_2 \cdot 4\text{H}_2\text{O}$, 98%, Aladdin), methanol (CH_3OH , $\geq 99.5\%$, Guangzhou Chemical Reagent), hydrobromic acid (HBr, 48 wt% in water, Aladdin), acetonitrile ($>99.5\%$, Aladdin), n-Hexane ($>99\%$, Aladdin), isopropyl alcohol (99.5%, Aladdin), anhydrous diethyl ether ($\geq 99.0\%$, Guangzhou Baijun Technology), ethanol (99.8%, Aladdin). The standard scintillator of Ce^{3+} -doped $\text{Lu}_3\text{Al}_5\text{O}_{12}$ (LuAG: Ce) crystal was purchased from EPIC Crystal Inc. All reagents were used as received without further purification.

Synthesis of 4-NH₃TBPBr single crystal.

The phosphonium bromide salt is synthesized according to the reference routes.¹ Typically, triphenylphosphine (10 mM), 4-bromo-1-butanamine hydrobromide (10 mM) and acetonitrile (15 ml) were added in a round bottom flask (100 mL). The resulting suspension was refluxed and stirred at 100 °C for 16 hours, and then hexane was added after the reaction was cooled to room temperature. The excess solvent was removed by rotary evaporation, and then the obtained viscous liquid was frozen in a refrigerator overnight. Finally, the obtained solid was recrystallized in ether and isopropanol solution to obtain a white solid powder with higher purity. ¹H NMR (400 MHz, DMSO-*d*₆) δ 7.92 (t, J = 7.2 Hz, 3H), 7.80 (m, 15H), 3.68 (t, J = 14.9 Hz, 2H), 2.92 – 2.77 (m, 2H), 1.80 (m, 2H), 1.73 – 1.54 (m, 2H). ³¹P NMR (400 MHz, DMSO-*d*₆) δ 24.14.

Synthesis of 4-DMATBPBr single crystal.

At room temperature, a solution of dimethylamine in water (40 wt%, 15 mL) was added to a suspension of (4-bromobutyl)triphenylphosphonium (10 mM) in ethanol (25 mL). The mixture was heated and refluxed at 100 °C for 6 h. After the reaction mixture was concentrated under reduced pressure, the solid residue was recrystallized in acetonitrile to obtain (4-(dimethylamino)butyl)triphenylphosphonium bromide hydrobromide as a white solid. ¹H NMR (400 MHz, Chloroform-*d*) δ 8.12 – 7.49 (m, 15H), 3.81 – 3.65 (m, 2H), 3.57 – 3.42 (m, 2H), 2.89 (s, 6H), 2.36 (m, 2H), 1.87 (m, 2H). ³¹P NMR (400 MHz, Chloroform-*d*) δ 24.09.

Synthesis of (4-NH₃TBP)MnBr₄ single crystal.

The (4-NH₃TBP)MnBr₄ crystals were prepared through a solvothermal method. In detail, the as-synthesized 4-NH₃TBPBr (1 mmol) and MnBr₄·4H₂O (1 mmol) were dissolved in CH₃OH (0.5 mL) solution. Then the precursor solution was transferred to a Teflon-lined stainless autoclave (10 mL) and kept at 100 °C for 6 h. The obtained solution was continuously evaporated at 120 °C to obtain green crystals.

Growth of (4-DMATBP)MnBr₄ single crystal.

In a typical synthesis procedure, 4-DMATBPBr (4 mmol) and MnBr₂·4H₂O (4 mmol) were dissolved in the mixed solution of CH₃OH (12 mL) and HBr (2 mL). The resulting mixture was filtered through a microporous nylon membrane with a pore size of 0.22 μm and then poured into an evaporating dish. Then, the solution was volatilized slowly for 3 days at 40 °C. Finally, the transparent yellow single crystals were obtained.

Preparation of (4-NH₃TBP)MnBr₄ and (4-DMATBP)MnBr₄ wafers.

Briefly, the (4-NH₃TBP)MnBr₄ and (4-DMATBP)MnBr₄ crystals were ground and pressed into wafers (100 MPa for 5 min). Due to the different degrees of hygroscopicity, the thickness of two wafers is difficult to keep the same. (4-NH₃TBP)MnBr₄ crystal shows high hygroscopicity, so it is challenging to completely demold from the mould due to the hydrogen bonding between –NH₃ in OIMH and water molecules in the air. As a result, the thickness of the wafer can only reach as thick as ~800 μm . Nevertheless, the thickness of (4-DMATBP)MnBr₄ wafer can be as thin as 500 μm , similar to that of single crystal due to weak hygroscopicity.

Single-crystal X-ray diffraction.

Single-crystal X-ray diffraction (SCXRD) measurements for 4-NH₃TBPBr, 4-DMATBPBr, (4-NH₃TBP)MnBr₄, and (4-DMATBP)MnBr₄ were performed on the Agilent Technologies Gemini A Ultra system at 150 K with Mo K α ($\lambda = 0.71073$ Å) radiation. The SCXRD data for the (4-DMATBP)MnBr₄ at different temperatures (303 K, 403 K, 473 K, and return to 303 K after heating) were collected under the same measurement condition, which was heated to the target temperature and kept for 15 minutes. The crystal structures were visualized using VESTA software.² Crystallographic data of as-synthesized crystals can be obtained for free in the Cambridge Crystallographic Data Centre (CCDC) with the accession number of 2379301-2379308.

Powder X-ray diffraction.

Room temperature powder X-ray diffraction (PXRD) measurement was carried out on Miniflex 600 diffractometer (Rigaku). Temperature-dependent PXRD measurement was performed on SmartLab diffractometer (Rigaku).

Thermal analysis.

Thermogravimetry analysis (TGA) was performed on Netzsch TG209F1 Libra instrument. The sample was heated from room temperature to 800 °C with a heating rate of 10 °C min⁻¹ under the N₂ flow. Differential scanning calorimetry (DSC) analysis was conducted on Netzsch DSC 214 instrument. The sample was heated at a heating rate of 20 °C min⁻¹ under the N₂ atmosphere.

Photoluminescent properties.

Room-temperature steady-state and time-resolved photoluminescence spectra were obtained with FLS980 and FLS1000 (Edinburgh Instruments LTD). Temperature-dependent photoluminescence spectra were acquired using the FLS980 and FLS1000 equipped with an Oxford OptistatDN2 optical cryostat. Photoluminescence quantum yields (PLQYs) were recorded on the Hamamatsu C9920 system. Temperature-dependent photoluminescence quantum yields were performed on the fluorescence quantum efficiency measurement system (XPQY-EQE) equipped with a temperature-controllable heating sample holder.

Ultraviolet-visible (UV-Vis) diffuse reflectance spectroscopy.

The UV-Vis spectra were recorded on a Shimadzu UV 3600 spectrophotometer equipped with an integrating sphere. BaSO₄ was used as a reference sample. The transmittance spectra of the single crystal and the wafer were measured in the range of 200–800 nm.

Fourier transform infrared (FTIR) spectroscopy.

The FTIR spectra were recorded using a PerkinElmer Frontier spectrophotometer. The data was collected using an attenuated total reflection (ATR) unit.

NMR spectra.

¹HNMR and ³¹PNMR spectra were recorded on a Varian Inova 400 MHz spectrometer (Bruker).

X-ray attenuation efficiency.

Attenuation efficiency (AE, %) demonstrates the attenuation capability of scintillators to X-rays and can be obtained from the following equation:³

$$\mu_{total} = \frac{\int_0^{E_{max}} \mu(E) \cdot N(E) dE}{\int_0^{E_{max}} N(E) dE}$$

$$AE = \left(1 - e^{-\mu_{total}\rho d}\right) \times 100\%$$

where $\mu(E)$ corresponds to the attenuation coefficient at the X-ray energy of E (keV) acquired from the XCOM database of National Institute Standards and Technology (NIST), $N(E)$ is the intensity at the X-ray energy of E (keV), E presents the X-ray energy, μ_{total} is the total attenuation coefficient; ρ and d refer to the density (g cm^{-3}) and thickness (cm).

RL and X-ray imaging measurement.

The RL spectra and their corresponding absolute photon number ($P_{measured}$) were collected by using an Ocean Optics portable spectrometer (QEpro) equipped with an integrating sphere. The X-ray tube with a silver (Ag) target (Amptek Mini-X2) was adopted as the X-ray source. The scintillator light yield was determined by using commercial LuAG:Ce as the reference with a standard light yield of 25,000 photon MeV^{-1} . The measured photon counts are normalized to 100 % X-ray attenuation by employing the following formula:³

$$P_{normalized} = \frac{P_{measured}}{AE(d)}$$

where $AE(d)$ denotes the attenuation efficiency (%) of sample at its thickness. The light yield can be calculated using the following equation:³

$$LY_{sample} = LY_{LuAG:Ce} \times \frac{P_{normalized}(Sample)}{P_{normalized}(LuAG:Ce)}$$

The photons emitted from the sample under different X-ray dose irradiation are collected by Hamamatsu H10721-210 photomultiplier tube. The limit of detection was determined as the dose rate when the signal-to-noise ratio (SNR) equals 3. The dose rate of the incident X-rays was adjusted by changing the X-ray tube current, and the dose rate was calibrated through the Radical X-ray dosimeter.

A self-built X-ray imaging system is constructed, as shown in Fig. 5f. The object and scintillator were placed under the incident X-rays. The X-ray images were captured by using a digital camera (Nikon D850).

Thermoluminescent (TL) spectrum.

TL was performed with an FJ-427A1 microcomputer TL dosimeter at a heating rate of 1 K s^{-1} from RT to $200 \text{ }^\circ\text{C}$. The sample was pre-irradiated under X-ray for 10 minutes.

Electron paramagnetic resonance (EPR) measurements.

EPR spectra were obtained with a commercial Bruker JES-FA200 in X-band (9.455 GHz) at room temperature.

EPR spectra simulations were performed through ‘‘Easyspin toolbox 6.0.0’’ package by using the fitting function as follows:

$$H = \beta g \hat{S} H + B_2^0 O_2^0 + B_2^2 O_2^2$$

where β , g , \hat{S} , and H represent Bohr magneton, g factor, spin operator (electron spin $S=5/2$ for Mn^{2+} , $3d^5$ outer shell), and magnetic field, B_2^n and O_2^n refer to crystal field parameters and Stevens operators.⁴

The fitting parameters are as follows: $g = 1.96$, $B_2^0 = 1157 \text{ MHz}$, $B_2^2 = 10 \text{ MHz}$.

DFT calculations.

All density functional theory computations were performed using the CP2K software package.⁵ PBE with Grimme D3 correction was employed in this system.^{6,7} Unrestricted Kohn-Sham DFT has been used as the electronic structure method in the framework of Gaussian and plane waves method.⁸ The Goedecker-Teter-Hutter (GTH) pseudopotentials and DZVP-MOLOPT-GTH basis sets were utilized to describe the molecules.⁹ Wavefunctions expanded in plane waves were cut off

to a 500 eV kinetic energy. The analyses of density of states (DOS) and projected DOS (PDOS) were performed on Multiwfn software.¹⁰

Table S1: The crystal structure data of 4-NH₃TBPBr, (4-NH₃TBP)MnBr₄, 4-DMATBPBr, and (4-DMATBP)MnBr₄.

Crystal	4-NH ₃ TBPBr	(4-NH ₃ TBP)MnBr ₄	4-DMATBPBr	(4-DMATBP)MnBr ₄
Formula	C ₂₂ H ₂₆ Br ₂ NP	C ₂₂ H ₂₆ Br ₄ MnNP	C ₂₄ H ₃₀ Br ₂ NP	C ₂₄ H ₃₀ Br ₄ MnNP
Formula weight	495.23	709.99	522.77	738.04
Temperature (K)			149.99	
Crystal system	orthorhombic	triclinic	monoclinic	monoclinic
Space group	Pna2 ₁	P $\bar{1}$	P2 ₁ /c	P2 ₁ /n
a (Å)	11.8011	8.5137	27.4156	13.0435
b (Å)	13.8575	12.2993	14.9303	11.7766
c (Å)	26.5401	12.7994	11.6527	18.3955
α (°)	90	105.646	90	90
β (°)	90	95.716	101.431	100.719
γ (°)	90	93.676	90	90
Volume (Å ³)	4340.20	1278.38	4675.10	2776.39
Z	8	2	8	4
ρ_{calc} (g cm ⁻³)	1.516	1.844	1.485	1.766
μ (mm ⁻¹)	3.815	6.840	3.546	6.302
F(000)	2000.0	690.0	2124.0	1440.0
Radiation		Mo K α ($\lambda = 0.71073$ Å)		
2 θ range for data collection (°)	4.786 to 54.206	4.830 to 65.902	4.960 to 54.206	4.698 to 50.050
Reflection collected	26678	35977	29466	11375
Independent reflections	8723	8800	10305	4897
Goodness-of-fit on F ²	1.050	1.037	1.028	1.029

Table S2: The thermal properties of the as-synthesized phosphonium salts.

Sample	T _m (°C)	T _g (°C)	T _d (°C)
4-NH ₃ TBPBr	166.6	97.4	255.0
4-DMATBPBr	262.1	60.0	275.0

Table S3: The Mn-Br bond lengths and shortest Mn-Mn distances of (4-NH₃TBP)MnBr₄ crystal and (4-DMATBP)MnBr₄ crystal.

Crystal	(4-NH ₃ TBP)MnBr ₄	(4-DMATBP)MnBr ₄
Mn1-Br1 (Å)	2.5486	2.5532
Mn1-Br2 (Å)	2.5238	2.5042
Mn1-Br3 (Å)	2.5152	2.4852
Mn1-Br4 (Å)	2.4755	2.4992
L _{ave} (Mn-Br) (Å)	2.5158	2.5105
Shortest Mn-Mn (Å)	6.6080	7.6060

Table S4: The thermal properties of the as-synthesized Mn-based halides.

Sample	T _m (°C)	T _g (°C)	T _d (°C)
(4-NH ₃ TBP)MnBr ₄	244.3	89.9	288.0
(4-DMATBP)MnBr ₄	262.0	88.8	314.0

Table S5: The Mn...H(Y)–C (N) bond lengths between [MnBr₄]²⁻ and organic cations in (4-NH₃TBP)MnBr₄ crystal.

Mn...H(Y) ^[a]	d (Å)
Mn1...H(A)	12.73
Mn1...H(B)	11.96
Mn1...H(C)	12.75
Mn1...H(D)	11.49
Mn1...H(E)	10.69
Mn1...H(F)	9.94
Mn1...H(G)	10.56
Mn1...H(H)	3.84
Mn1...H(I)	6.94
Mn1...H(J)	4.53
Mn1...H(K)	3.94
Mn1...H(L)	9.10
Mn1...H(M)	8.31
Mn1...H(N)	7.72
Mn1...H(O)	5.39
Mn1...H(P)	4.35
Mn1...H(Q)	5.69
Mn1...H(R)	8.63
Mn1...H(S)	7.97
Mn1...H(T)	8.92
Mn1...H(U)	6.87
Mn1...H(V)	6.19
Mn1...H(W)	7.75
Mn1...H(X)	7.02
Mn1...H(Y)	9.62
Mn1...H(Z)	9.97

^[a] Y refers to the serial number of H atom in organic cations.

Table S6: The Mn...H(Y)–C (N) bond lengths between [MnBr₄]²⁻ and organic cations in (4-DMATBP)MnBr₄ crystal.

Mn(X) ^[a] ...H(Y) ^[b]	d (Å)	Mn(X)...H(Y)	d (Å)	Mn(X)...H(Y)	d (Å)	Mn(X)...H(Y)	d (Å)
Mn1...H3	11.93	Mn2...H4	11.93	Mn3...H1	7.43	Mn4...H2	7.43
Mn1...H7	11.84	Mn2...H8	11.84	Mn3...H5	7.44	Mn4...H6	7.44
Mn1...H11	9.56	Mn2...H12	9.55	Mn3...H9	3.51	Mn4...H10	3.51
Mn1...H15	9.28	Mn2...H16	9.27	Mn3...H13	4.83	Mn4...H14	4.83
Mn1...H19	10.15	Mn2...H20	10.14	Mn3...H17	3.93	Mn4...H18	3.93
Mn1...H23	6.77	Mn2...H24	6.76	Mn3...H21	7.95	Mn4...H22	7.95
Mn1...H27	11.57	Mn2...H28	11.57	Mn3...H25	5.05	Mn4...H26	5.05
Mn1...H31	11.95	Mn2...H32	11.95	Mn3...H29	4.88	Mn4...H30	4.88
Mn1...H35	10.55	Mn2...H36	10.54	Mn3...H33	5.17	Mn4...H34	5.17
Mn1...H39	6.60	Mn2...H40	6.60	Mn3...H37	7.35	Mn4...H38	7.35
Mn1...H43	6.12	Mn2...H44	6.12	Mn3...H41	10.78	Mn4...H42	10.77
Mn1...H47	9.90	Mn2...H48	9.90	Mn3...H45	6.42	Mn4...H46	6.42
Mn1...H51	9.45	Mn2...H52	9.45	Mn3...H49	6.68	Mn4...H50	6.68
Mn1...H55	5.27	Mn2...H56	5.26	Mn3...H53	7.86	Mn4...H54	7.86
Mn1...H59	11.68	Mn2...H60	11.67	Mn3...H57	6.68	Mn4...H58	6.68
Mn1...H63	7.23	Mn2...H64	7.22	Mn3...H61	8.60	Mn4...H62	8.60
Mn1...H67	7.95	Mn2...H68	7.94	Mn3...H65	6.92	Mn4...H66	6.92
Mn1...H71	4.97	Mn2...H72	4.98	Mn3...H69	11.29	Mn4...H70	11.29
Mn1...H75	5.51	Mn2...H76	5.49	Mn3...H73	8.30	Mn4...H74	8.30
Mn1...H79	5.35	Mn2...H80	5.36	Mn3...H77	9.81	Mn4...H78	9.81
Mn1...H83	9.68	Mn2...H84	9.67	Mn3...H81	4.44	Mn4...H82	4.44
Mn1...H87	14.18	Mn2...H88	14.18	Mn3...H85	8.82	Mn4...H86	8.82
Mn1...H91	15.41	Mn2...H92	15.41	Mn3...H89	8.70	Mn4...H90	8.70
Mn1...H95	14.20	Mn2...H96	14.20	Mn3...H93	9.02	Mn4...H94	9.02
Mn1...H99	8.46	Mn2...H100	8.44	Mn3...H97	9.01	Mn4...H98	9.01
Mn1...H103	10.79	Mn2...H104	10.77	Mn3...H101	8.49	Mn4...H102	8.49
Mn1...H107	13.92	Mn2...H108	13.93	Mn3...H105	7.29	Mn4...H106	7.29
Mn1...H111	15.16	Mn2...H112	15.16	Mn3...H109	7.01	Mn4...H110	7.01
Mn1...H115	13.68	Mn2...H116	13.68	Mn3...H113	5.57	Mn4...H114	5.57
Mn1...H119	13.88	Mn2...H120	13.88	Mn3...H117	6.57	Mn4...H118	6.57

^[a] X is the serial number of Mn atom in [MnBr₄]²⁻ anions; ^[b] Y refers to the serial number of H atom in organic cations.

Table S7: The crystal structure data of (4-DMATBP)MnBr₄ crystal at different temperatures.

Temperature (K)	303	403	473	303 (2 nd) [a]
Formula weight			738.04	
Crystal system			monoclinic	
Space group			P2 ₁ /n	
a (Å)	13.0431	13.0324	13.0107	13.0405
b (Å)	11.9668	12.1492	12.3135	11.9672
c (Å)	18.5423	18.6523	18.7294	18.5389
α (°)	90	90	90	90
β (°)	100.809	100.893	101.032	100.787
γ (°)	90	90	90	90
Volume (Å ³)	2842.81	2900.1	2945.1	2842.03
Z			4	
ρ_{calc} (g cm ⁻³)	1.722	1.688	1.644	1.723
μ (mm ⁻¹)	6.155	6.033	5.941	6.157
F(000)			1440.0	
Radiation			Mo K α (λ = 0.71073 Å)	
2 Θ range for data collection (°)	4.658 to 55.824	4.622 to 55.812	4.596 to 50.054	4.658 to 55.836
Reflection collected	13452	13703	12215	13449
Independent reflections	6269	6387	5210	6266
Goodness-of-fit on F ²	1.018	0.964	0.999	1.002

[a] The data collected at 303 K(2nd) presents the crystal structure cooled to 303 K after being heated to 473 K.

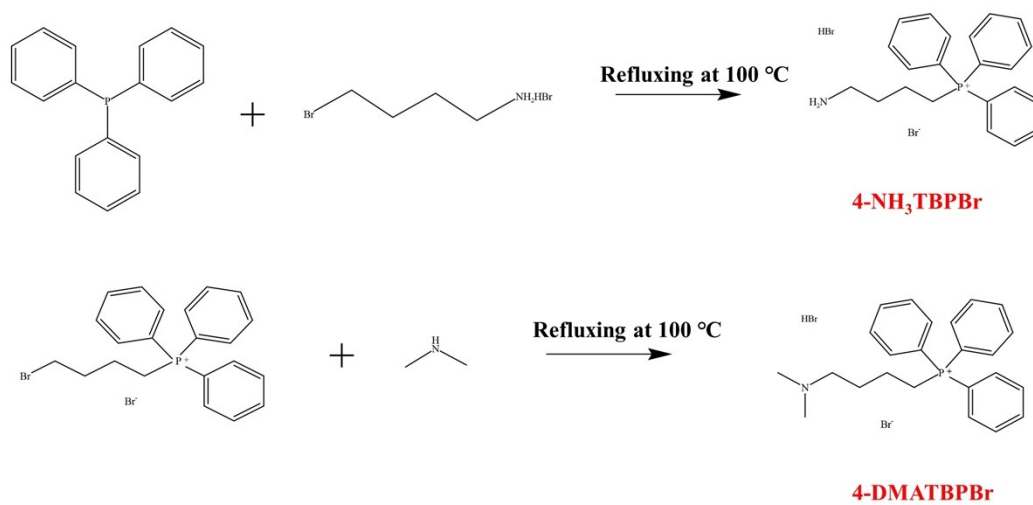
Table S8: The crystal volume and shortest Mn-Mn distance of (4-DMATBP)MnBr₄ crystal at different temperatures.

Temperature (K)	Volume (Å ³)	Shortest Mn-Mn distance (Å)
303	2842.81	7.759
403	2900.10	7.927
473	2945.10	8.103
303 (2 nd) ^[a]	2842.03	7.762

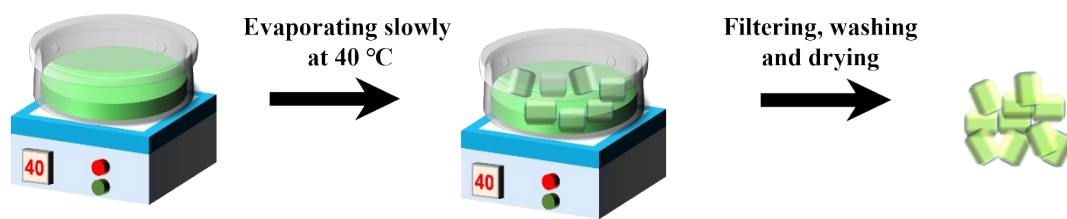
^[a] The data collected at 303 K(2nd) presents the crystal structure cooled to 303 K after being heated to 473 K.

Table S9: The average PL lifetimes of (4-DMATBP)MnBr₄ crystal at different temperatures.

Temperature (K)	τ_{ave} (μs)
303	125
313	97
323	90
333	91
343	98
353	105
363	128
373	163
383	238
403	254
423	238
443	207
463	165
473	139



Supplementary Scheme 1: Synthesis routes of 4-NH₃TBPBr and 4-DMATBPBr crystals.



Supplementary Scheme 2: Schematic diagram of the synthesis route of large-size (4-DMATBP)MnBr₄ single crystal.

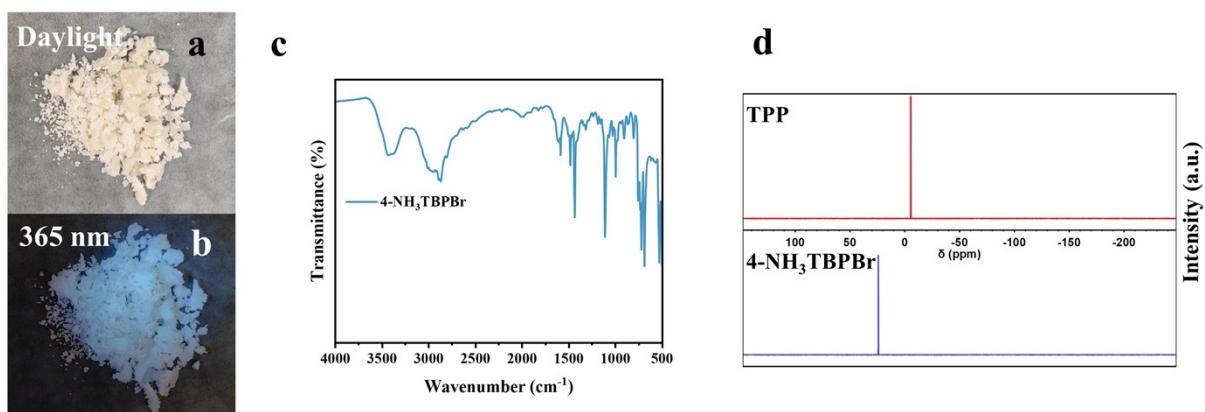


Fig. S1: Physical characterization of the as-synthesized 4-NH₃TBPBr crystal. Photograph of 4-NH₃TBPBr crystal (a) under sunlight and (b) under 365-nm ultraviolet light. (c) Attenuated total reflectance (ATR)-Fourier transform infrared spectrum of 4-NH₃TBPBr. (d) ³¹P NMR spectra of 4-NH₃TBPBr.

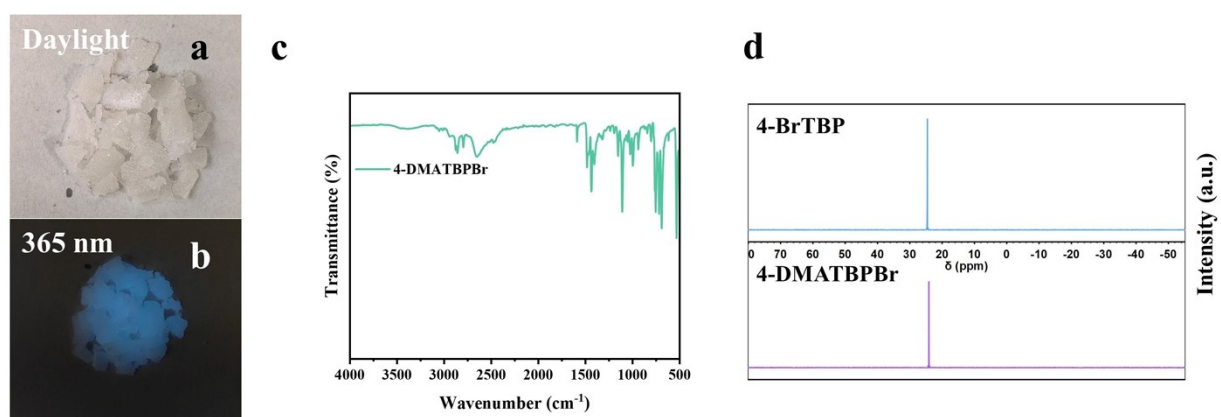


Fig. S2: Physical characterization of the as-synthesized 4-DMATBPBr crystal. Photograph of 4-DMATBPBr crystal (a) under sunlight and (b) under 365-nm ultraviolet light. (c) Attenuated total reflectance (ATR)-Fourier transform infrared spectrum of 4-DMATBPBr. (d) ³¹P NMR spectra of 4-DMATBPBr.

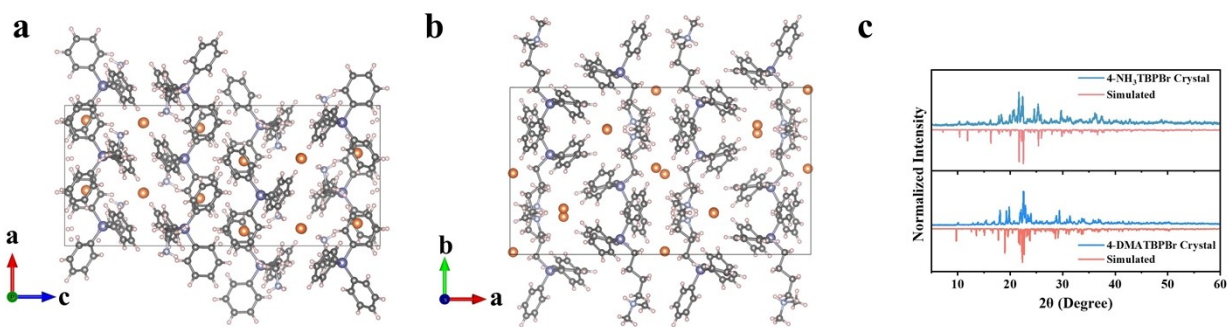


Fig. S3: Single-crystal structure of the as-synthesized organic compounds. Crystal structure of (a) 4-NH₃TBPBr and (b) 4-DMATBPBr crystal (pink: H, grey: C, light purple: N, orange: Br, purple: P). (c) Comparison of the simulated XRD and experimental XRD patterns of 4-NH₃TBPBr and 4-DMATBPBr crystal.

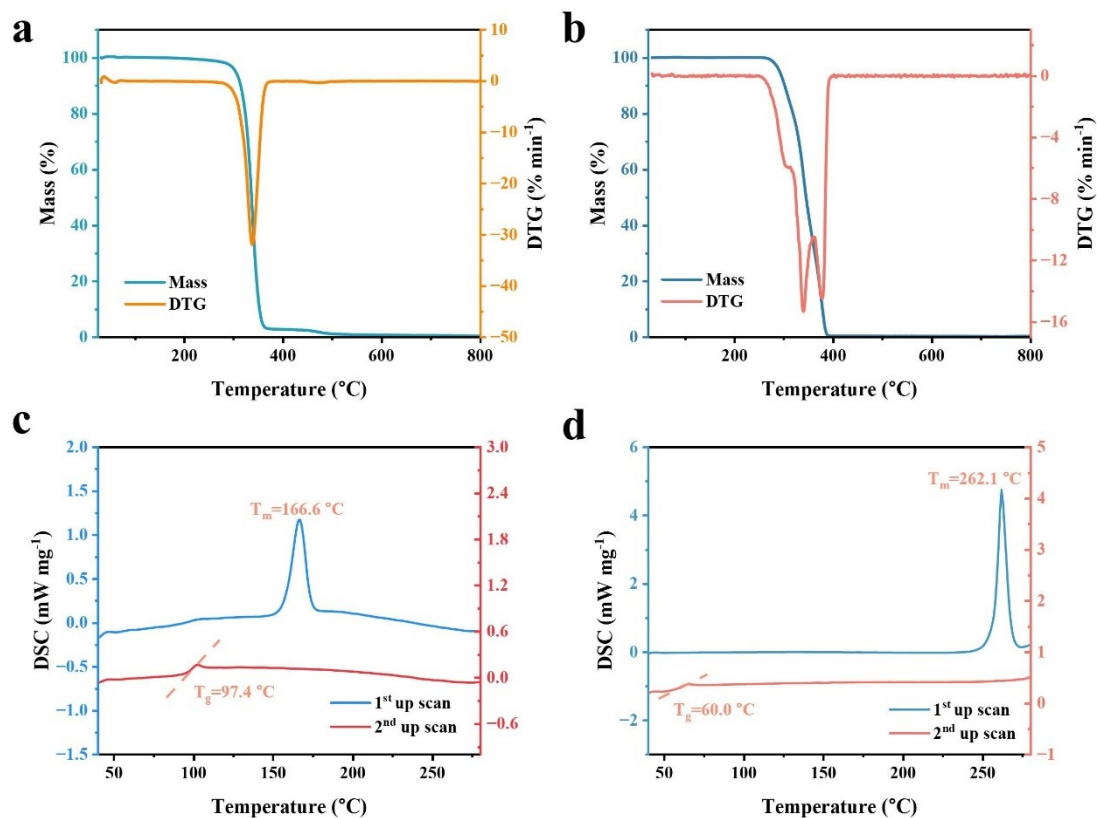


Fig. S4: Thermal properties of the as-synthesized phosphonium salts. (a) TG and (c) DSC plots of 4-NH₃TBPBr. (b) TG and (d) DSC plots of 4-DMATBPBr.

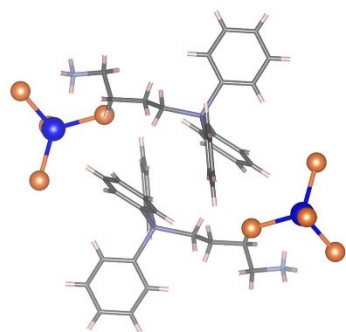
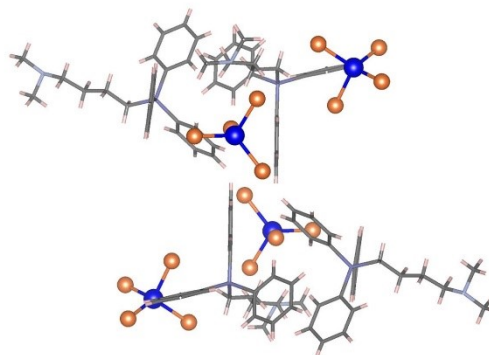
a**b**

Fig. S5: The asymmetric units of (a) (4-NH₃TBP)MnBr₄ and (b) (4-DMATBP)MnBr₄ crystal; H atoms are removed for clarity.

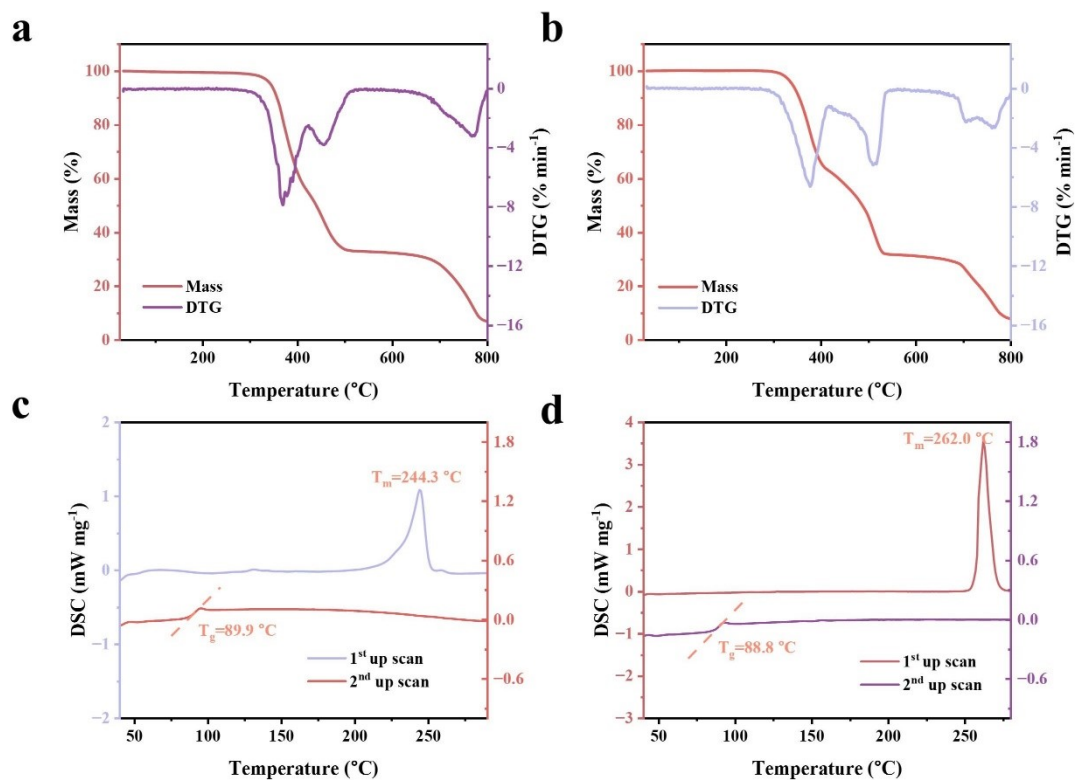


Fig. S6: Thermal properties of the as-synthesized metal halide crystals. (a) TG and (c) DSC plots of (4-NH₃TBP)MnBr₄. (b) TG and (d) DSC plots of (4-DMATBP)MnBr₄.

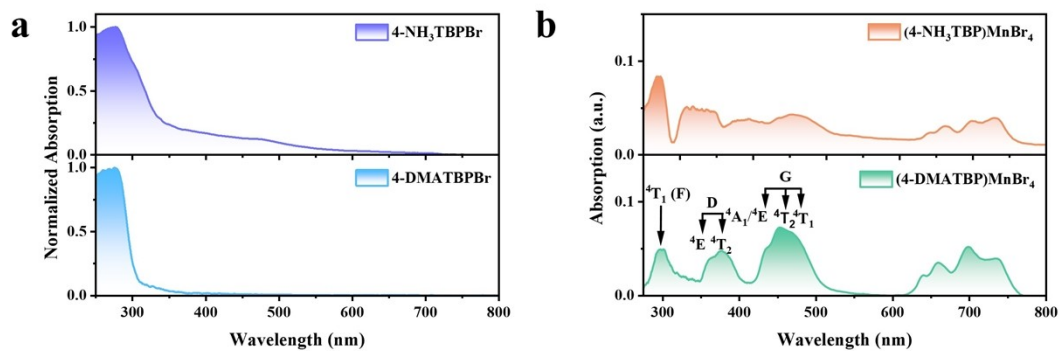


Fig. S7: Optical properties of as-synthesized compounds. (a) UV-Vis spectra of 4-NH₃TBPBr and 4-DMATBPBr compounds. (b) UV-Vis spectra of (4-NH₃TBP)MnBr₄ and (4-DMATBP)MnBr₄ crystal.

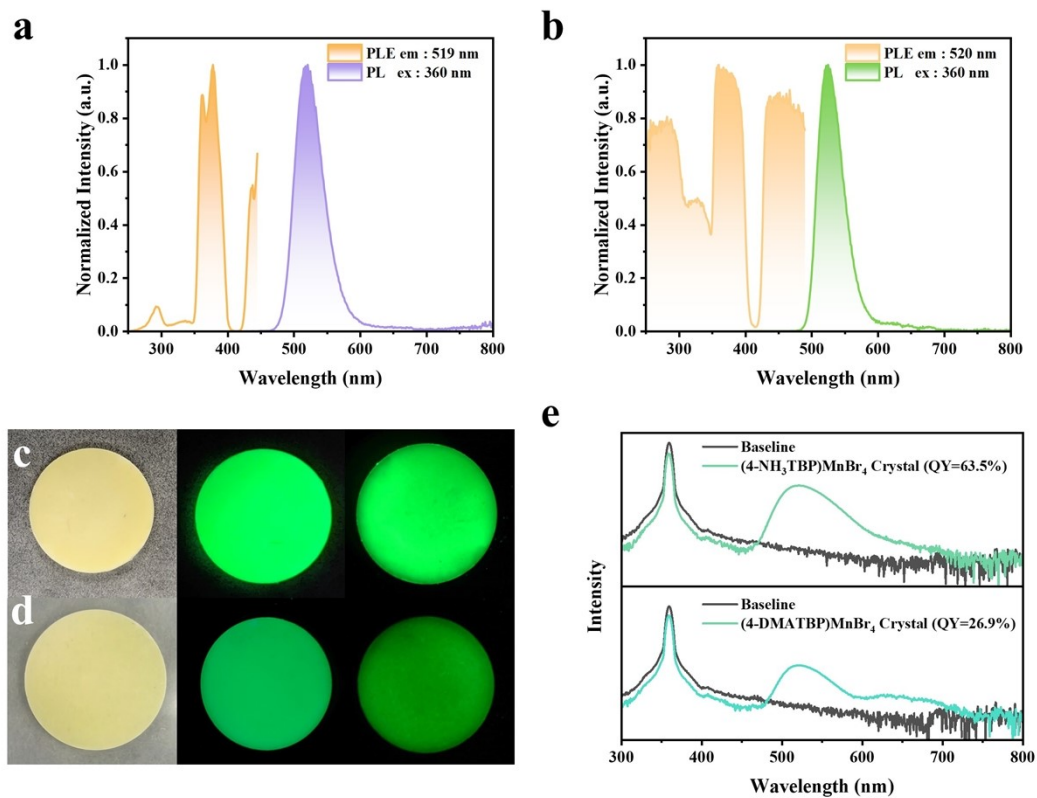


Fig. S8: Photoluminescence properties of the as-synthesized Mn-based crystal. Excitation and emission spectra of crystalline (a) (4-NH₃TBP)MnBr₄ and (b) (4-DMATBP)MnBr₄ crystal. Photographs of (c) (4-NH₃TBP)MnBr₄ and (d) (4-DMATBP)MnBr₄ wafer under sunlight, 365 nm ultraviolet, and X-ray from left to right. (e) PLQY plots of (4-NH₃TBP)MnBr₄ and (4-DMATBP)MnBr₄ crystal.

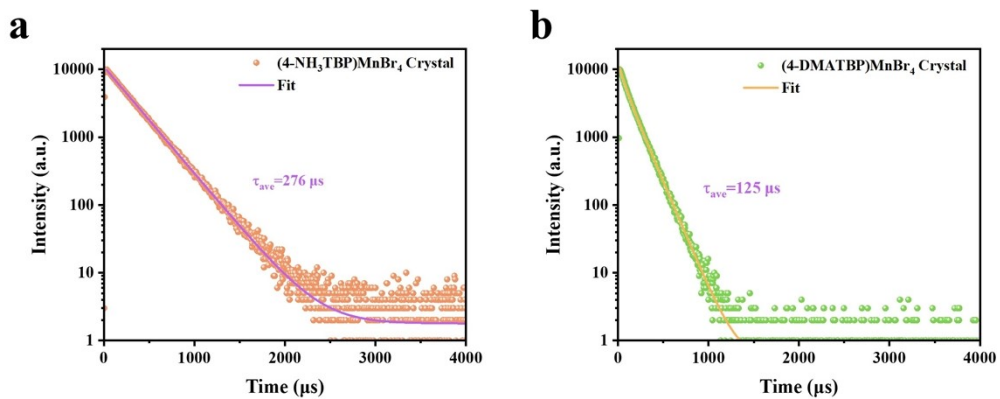


Fig. S9: The decay lifetime of two single crystals. Time-resolved photoluminescence decay curves of (a) (4-NH₃TBP)MnBr₄ and (b) (4-DMATBP)MnBr₄ crystal.

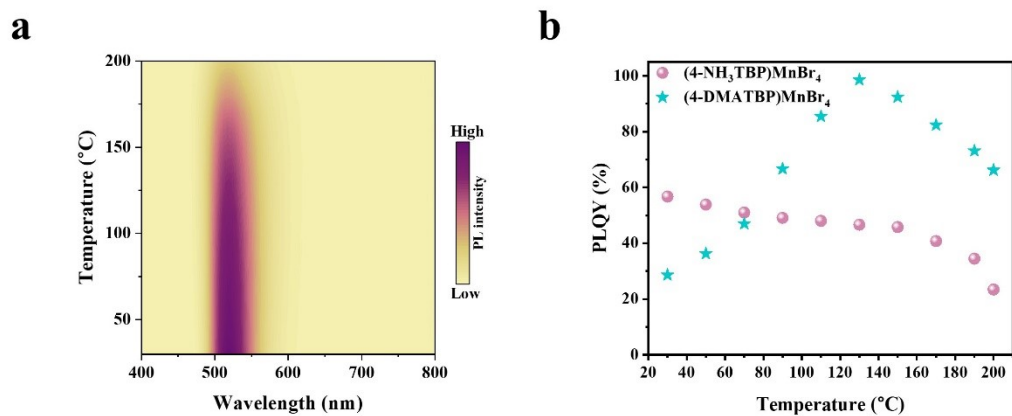


Fig. S10: Photoluminescence properties and PLQY of Mn-based crystals. (a) Temperature-dependent PL spectrum of (4-NH₃TBP)MnBr₄ crystal. (b) Temperature-dependent PLQY values of (4-NH₃TBP)MnBr₄ and (4-DMATBP)MnBr₄ crystal.

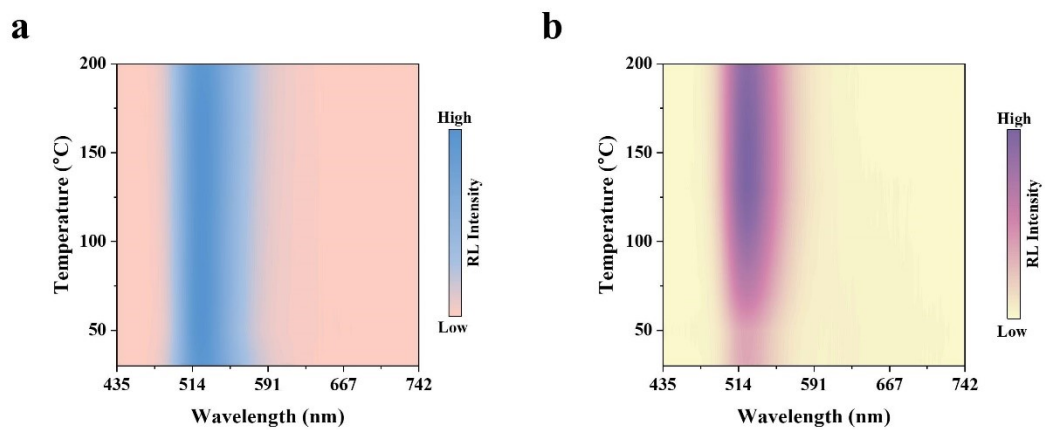


Fig. S11: Temperature-dependent RL spectrum of (a) (4-NH₃TBP)MnBr₄ crystal and (b) (4-DMATBP)MnBr₄ crystal.

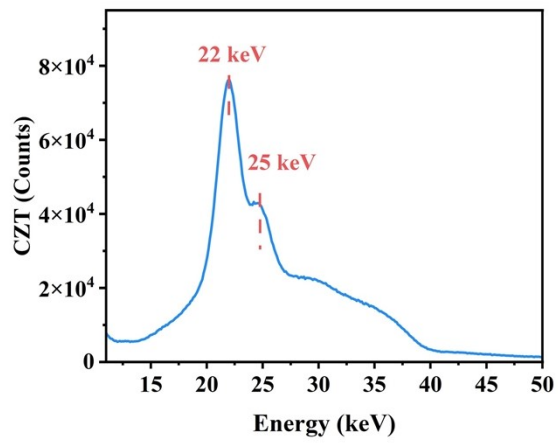


Fig. S12: The Mini-X2 silver (Ag) output spectrum collected at 40 kV.

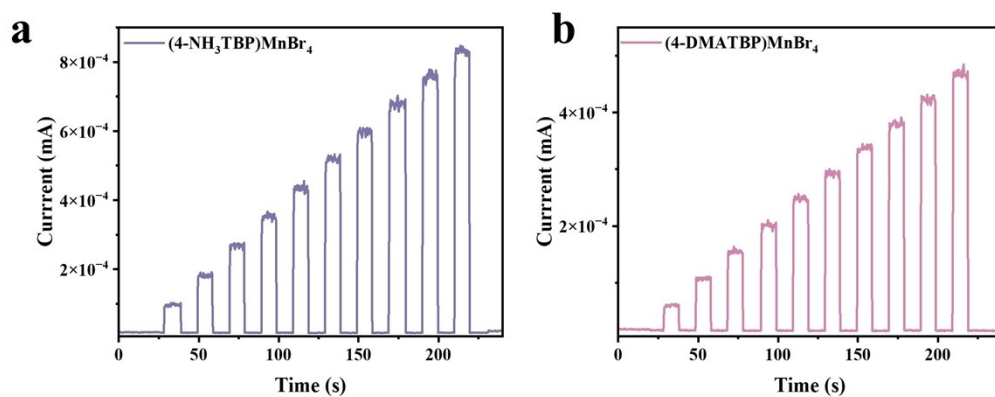


Fig. S13: RL response under different X-ray dose rates. The photomultiplier's response currents of (a) (4-NH₃TBP)MnBr₄ and (b) (4-DMATBP)MnBr₄ versus X-ray dose rate.

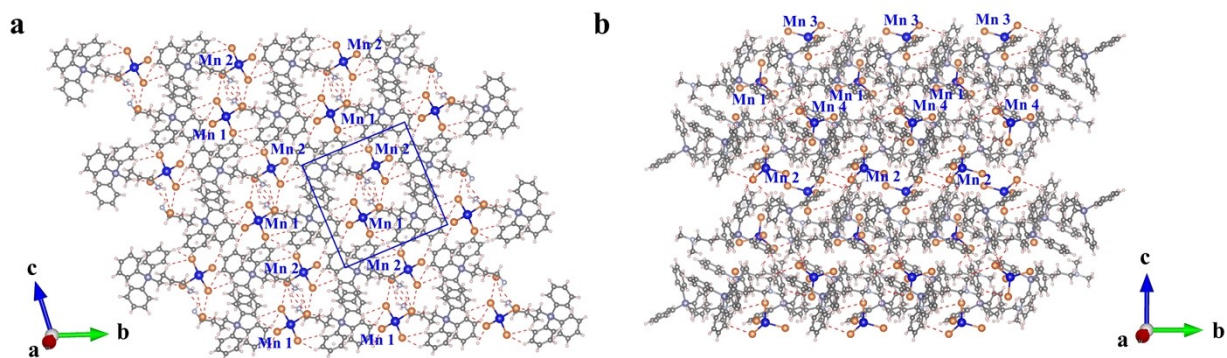


Fig. S14: 3D packing diagrams for (a) (4-NH₃TBP)MnBr₄ and (b) (4-DMATBP)MnBr₄ crystal viewed along the a-axis. C–H...Br H-bonds are shown in the red dashed lines. The blue box in (a) shows the fully ordered structure of (4-NH₃TBP)MnBr₄ crystal where the surrounding cations form a regular square configuration. Thus, the motion freedom of anions decreases.

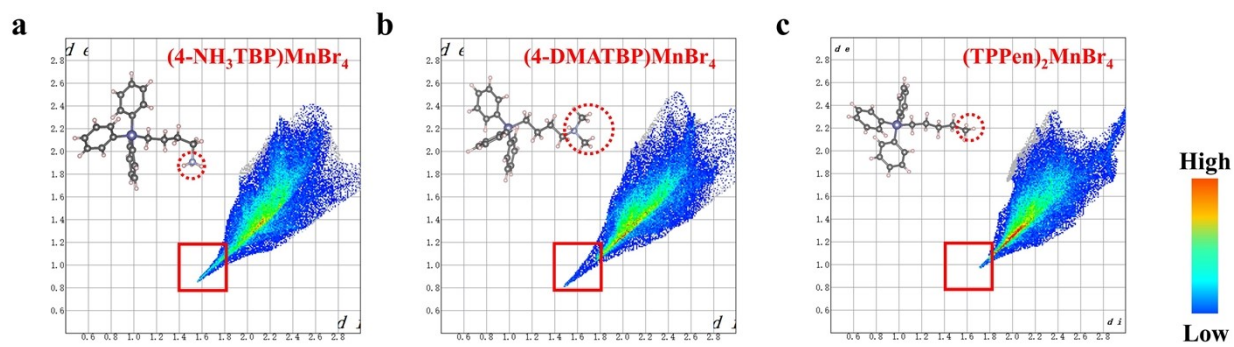


Fig. S15: The 2D fingerprint patterns for C–H...Br H-bond of $[\text{MnBr}_4]^{2-}$ in (a) $(4\text{-NH}_3\text{TBP})\text{MnBr}_4$, (b) $(4\text{-DMATBP})\text{MnBr}_4$, and (c) $(\text{TPPen})_2\text{MnBr}_4$ crystal.

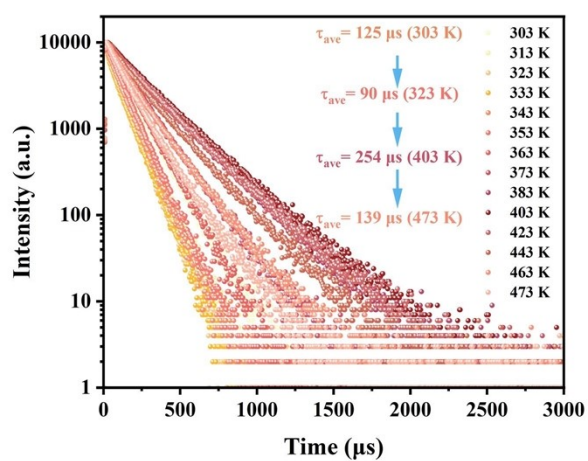


Fig. S16: Temperature-dependent PL decay curves of (4-DMATBP)MnBr₄ crystal (λ_{ex} =360 nm, λ_{em} =520 nm).

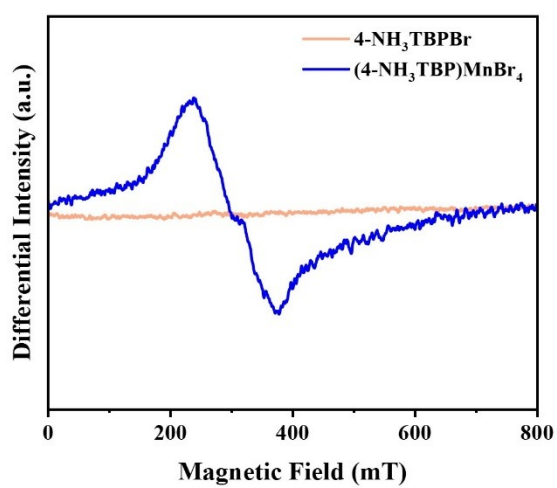


Fig. S17: EPR spectra of 4-NH₃TBPBr and (4-NH₃TBP)MnBr₄ crystal.

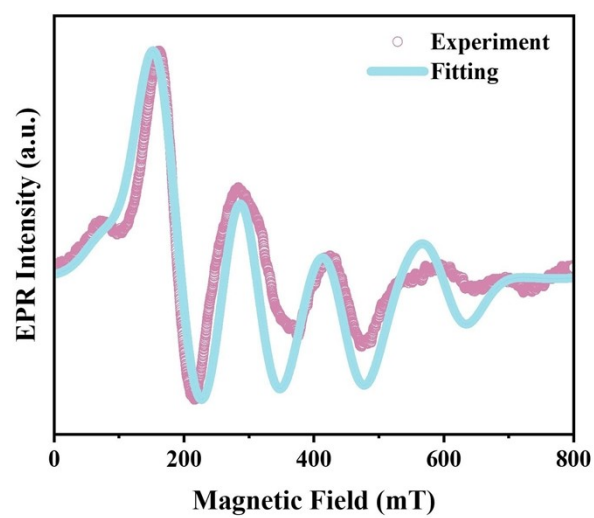


Fig. S18: Experimental and the fitted plot of EPR spectra for (4-DMATBP)MnBr₄ single crystal.

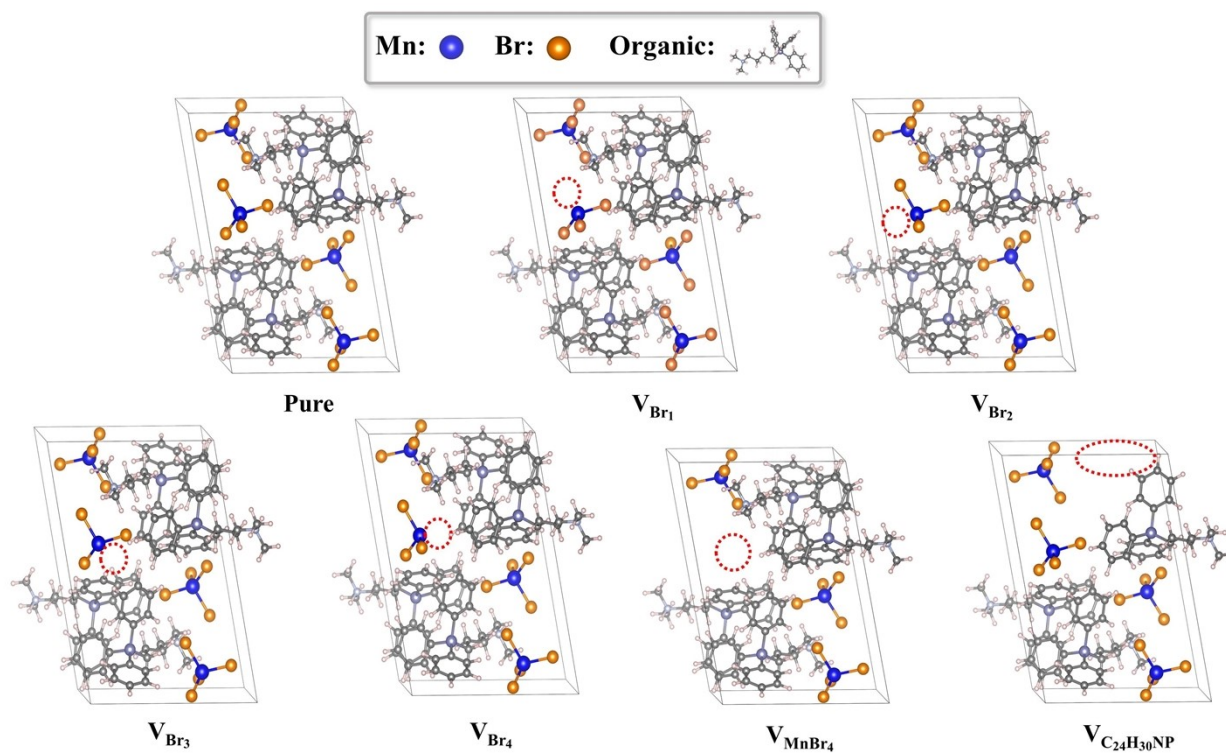


Fig. S19: Schematic diagram of the possible vacancy-defect structures in (4-DAMTBP) MnBr_4 crystal (Br, MnBr_4^{2-} , Organic).

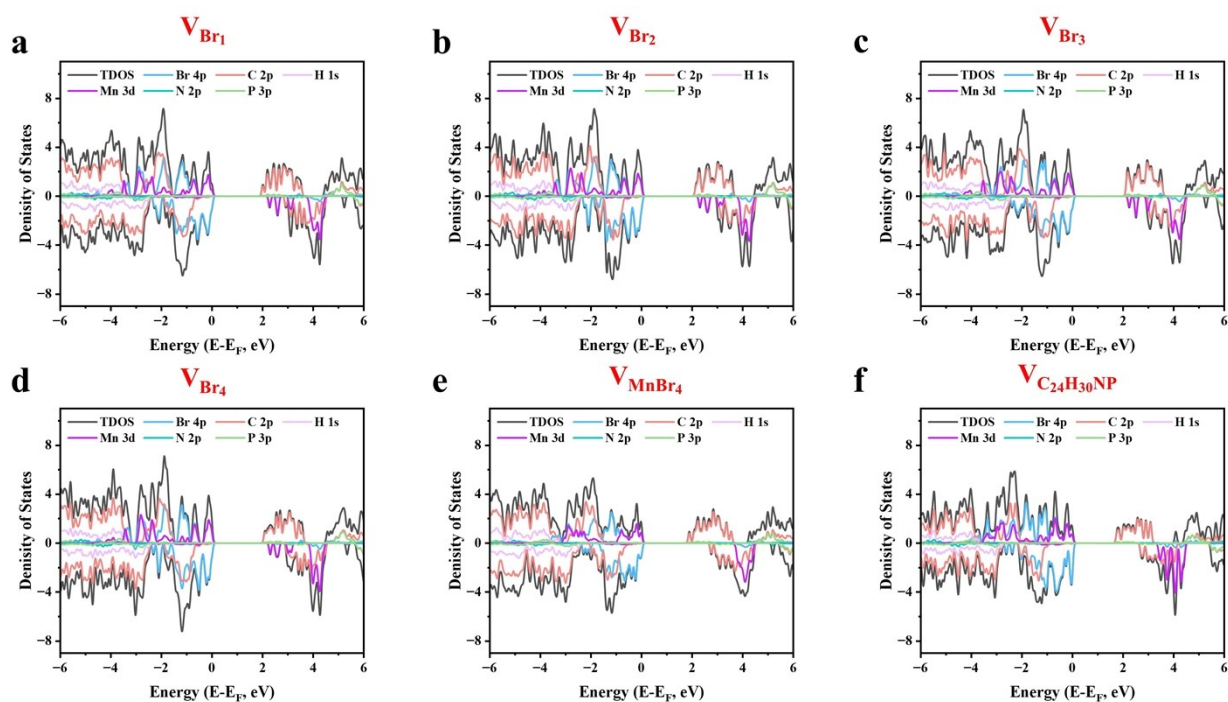


Fig. S20: The density of states and projected density of states of (4-DMATBP)MnBr₄ crystal with different structure defects. (a-d) The DOS plots of four different Br-vacancy, (e) [MnBr₄]²⁻ vacancy, and (f) organic vacancy structures.

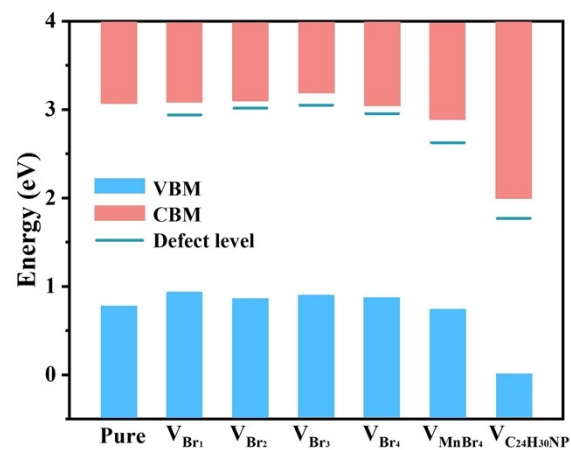


Fig. S21: Energy level diagram of pure (4-DAMTBP)MnBr₄ crystal and possible vacancy defects (shallow trap level).

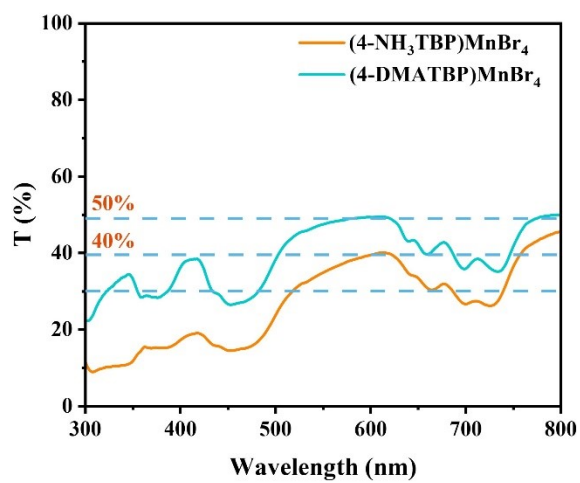


Fig. S22: Ultraviolet-visible transmittance spectra of (4-NH₃TBP)MnBr₄ and (4-DMATBP)MnBr₄ wafers.

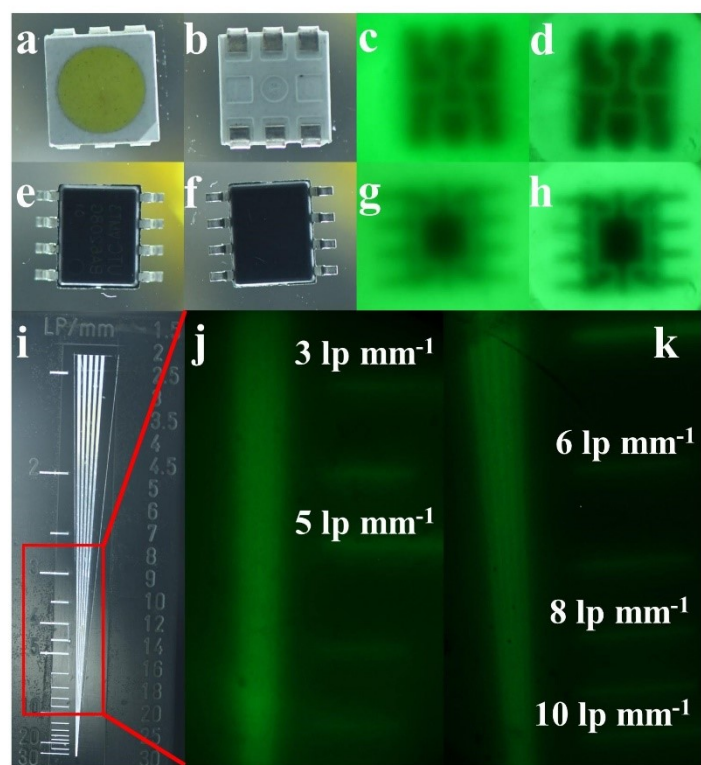


Fig. S23: X-ray imaging of the wafers. (a) The front and (b) back pictures of electronic component A. The X-ray images of (c) (4-NH₃TBP)MnBr₄ wafer and (d) (4-DMATBP)MnBr₄ wafer. (e) The front and (f) back pictures of electronic component B. The X-ray images of (g) (4-NH₃TBP)MnBr₄ wafer and (h) (4-DMATBP)MnBr₄ wafer. (i) Photograph of the line pair card. X-ray images of (j) (4-NH₃TBP)MnBr₄ and (k) (4-DMATBP)MnBr₄ wafers.

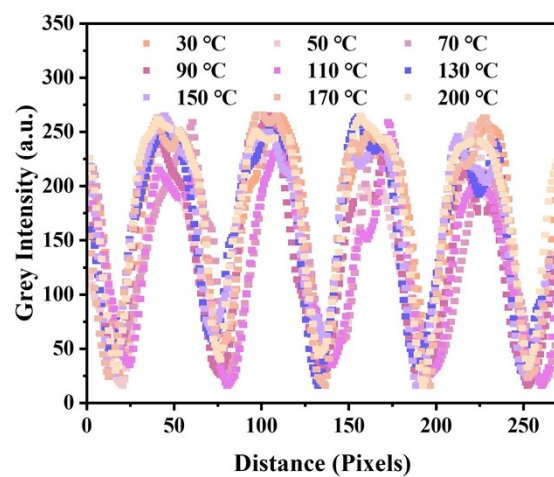


Fig. S24: The gray value changes of the X-ray imaging of the (4-DMATBP)MnBr₄ crystal along the dotted line in Fig. 5e at different temperatures.

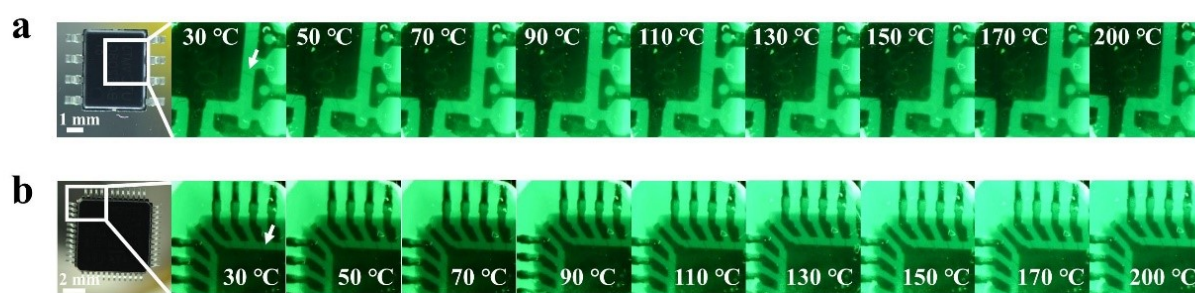


Fig. S25: X-ray images of (a) electronic component B and (b) electronic chip using the (4-DMATBP)MnBr₄ crystal at different temperatures. The arrow shows the details of the internal structure, and the width of the wire pointed in (a) and (b) are about 13 μm and 22 μm.

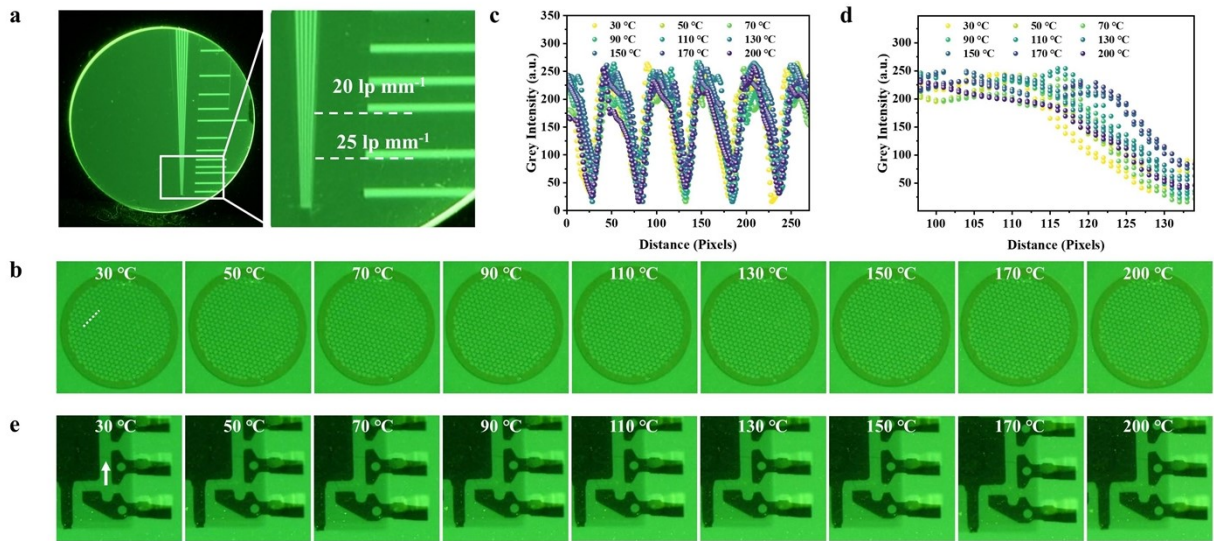


Fig. S26: X-ray imaging of LuAG:Ce scintillator. (a) X-ray imaging of a lead-made line pair card at room temperature. (b) Temperature-dependent X-ray images of a copper mesh (rib pitch: 20 μm). (c-d) The grey value changes of the X-ray imaging of the LuAG:Ce scintillator along the dotted line in (b) at different temperatures. (e) X-ray images of electronic component B using LuAG:Ce scintillator at different temperatures. The arrow shows the details of the internal structure, and the width of the wire pointed in (e) is 13 μm .

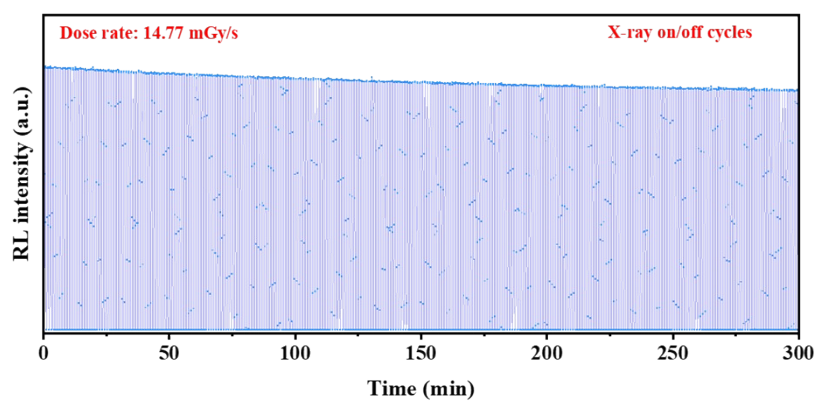


Fig. S27: The irradiation stability of (4-DMATBP)MnBr₄ crystal under X-ray irradiation with a total dosage of 133 Gy.

References

1. M. Millard, J.-D. Gallagher, B.-Z. Olenyuk, N. Neamati. *J. Med, Chem.*, 2013, **56**, 9170.
2. K. Momma, F. Izumi, *J. Appl. Crystallogr.*, 2011, **44**, 1272.
3. T. Jiang, W. Ma, H. Zhang, Y. Tian, G. Lin, W. Xiao, X. Yu, J. Qiu, X. Xu, *Adv. Funct. Mater.*, 2021, **31**, 2009973.
4. S. Stoll, A. Schweiger, *J. Magn. Reson.*, 2006, **178**, 42.
5. J. Hutter, M. Iannuzzi, F. Schiffmann, J. VandeVondele, *WIREs Comput Mol Sci.*, 2014, **4**, 15.
6. J.-P. Perdew, K. Burke, M. Ernzerhof, *Phys. Rev. Lett.*, 1996, **77**, 3865.
7. S. Grimme, *J. Comput. Chem.*, 2006, **27**, 1787.
8. J. VandeVondele, M. Krack, F. Mohamed, M. Parrinello, T. Chassaing, J. Hutter, *Comput. Phys. Commun.*, 2005, **167**, 103.
9. S. Goedecker, M. Teter, J. Hutter, *Phys. Rev. B*, 1996, **54**, 1703.
10. T. Lu, F. Chen, *J. Comput. Chem.*, 2012, **33**, 580.